IEEE Access
Multidisciplinary : Rapid Review : Open Access Journal

Received 7 January 2024, accepted 17 January 2024, date of publication 22 January 2024, date of current version 30 January 2024.

Digital Object Identifier 10.1109/ACCESS.2024.3357092

RESEARCH ARTICLE

Bilinear Double-Order Filter Designs and Application Examples

JULIA NAKO[1], **(Graduate Student Member, IEEE), COSTAS PSYCHALINOS**[1], **(Senior Member, IEEE), FABIAN KHATEB**[2,3,4], **AND AHMED S. ELWAKIL**[5,6,7], **(Senior Member, IEEE)**

[1]Department of Physics, Electronics Laboratory, University of Patras, Rio, 265 04 Patras, Greece
[2]Department of Microelectronics, Brno University of Technology, 601 90 Brno, Czech Republic
[3]Faculty of Biomedical Engineering, Czech Technical University in Prague, 272 01 Kladno, Czech Republic
[4]Department of Electrical Engineering, University of Defense, 662 10 Brno, Czech Republic
[5]Department of Electrical Engineering, University of Sharjah, Sharjah, United Arab Emirates
[6]Department of Electrical and Software Engineering, University of Calgary, Alberta, AB T2N 1N4, Canada
[7]Nanoelectronics Integrated Systems Center (NISC), Nile University, Giza 12677, Egypt

Corresponding author: Costas Psychalinos (cpsychal@upatras.gr)

This work was supported by HEAL-Link.

ABSTRACT A novel kind of non-integer order bilinear filters, named double-order bilinear filters, is introduced in this work. They are based on the employment of two non-integer orders, offering the maximum design flexibility in comparison with their fractional-order and power-law counterparts. An attractive offered benefit is that this is achieved without increasing the circuit complexity, since the proposed structure is capable of realizing all non-integer kinds of filters. Two design examples are provided, where it is shown that lead/lag compensators utilized in control applications and low/high shelving filters employed in acoustic applications are actually bilinear filters with suitably selected pole/zero frequencies. Simulation and experimental results, using the OrCAD PSpice simulator and a Field Programmable Analog Array device, respectively, support the findings of this work.

INDEX TERMS Analog filters, bilinear filters, compensators, curve-fitting approximation, field programmable analog array, fractional-order filters, power-law filters, shelving filters.

I. INTRODUCTION

The term "bilinear filter" is used for the characterization of filters which are expressed as a ratio of two linear functions. The transfer function of a first-order bilinear filter is

$$H_{IO}(s) = G_L \cdot \frac{y\tau s + 1}{x\tau s + 1}, \tag{1}$$

with $x, y > 0$ being dimensionless scaling factors, τ being a time constant, and G_L being the low-frequency gain of the filter.

Employing fractional calculus, the transfer function of a fractional-order bilinear filter is

$$H_{FO}(s) = G_L \cdot \frac{y(\tau s)^{\alpha} + 1}{x(\tau s)^{\alpha} + 1}, \tag{2}$$

with $0 < \alpha < 1$ being the order of the filter.

The transfer function of a power-law bilinear filter of order $0 < \beta < 1$ is given by

$$H_{PL}(s) = G_L \cdot \left(\frac{y\tau s + y_0}{x\tau s + x_0}\right)^{\beta}. \tag{3}$$

Meanwhile, the standard first-order low-pass and high-pass filter functions are directly derived from (1), by setting $y = 0$ and $x = y$, respectively.

Forms of fractional-order bilinear filter functions have been realized in [1], [2], [3], and [4], while the corresponding realization of power-law ones have been presented in [3]. Both the aforementioned kinds of filters offer improved design flexibility with regards to their integer-order counterparts, because of the variable non-integer order of the filters, which allows the adjustment of the main characteristics of their frequency behavior.

The associate editor coordinating the review of this manuscript and approving it for publication was Andrea De Marcellis.

© 2024 The Authors. This work is licensed under a Creative Commons Attribution-NonCommercial-NoDerivatives 4.0 License.
For more information, see https://creativecommons.org/licenses/by-nc-nd/4.0/

In this work, a double-order bilinear filter function is introduced where two degrees of freedom are offered because of the employment of two orders, instead of a single order in fractional-order and power-law filters. This enables having full control of the characteristics of the filter. This work is an extension of the work presented in [5]. Two possible implementations are demonstrated, with the first one based on the employment of a single Current Feedback Operational Amplifier (CFOA) as the active element, which also offers the capability of realizing all non-integer order functions by the same RC network, and just adjusting the values of resistors and capacitors. The second implementation is based on the utilization of a Field Programmable Analog Array (FPAA) device, which offers design programmability and versatility in the sense that all kinds of (non-integer order) bilinear filters can be implemented by re-programming the characteristics of the intermediate stages.

This work is organized as follows: a systematic review of the bilinear filter transfer functions, presented in the literature, is performed in Section II. The proposed generalized bilinear filter transfer function is introduced in Section II, where its possible implementations are also discussed. Two application examples are provided in Section IV, and the evaluation of the performance of the resulting schemes is performed through simulation results, obtained with the employment of the OrCAD PSpice suite and through experimental results using the FPAA AN231E04 device from Anadigm [6].

II. BILINEAR FILTER TRANSFER FUNCTIONS

A. INTEGER-ORDER BILINEAR FILTERS

Considering the expression in (1), the time constant is associated with a characteristic frequency ω_0 according to the formula: $\tau = 1/\omega_0$, and the pole and the zero are located in the left-half of the s-plane with their magnitudes being

$$\omega_p = \frac{1}{x\tau} = \frac{\omega_0}{x}, \quad \omega_z = \frac{1}{y\tau} = \frac{\omega_0}{y}. \tag{4}$$

According to (4), the pole (ω_p) and zero (ω_z) frequencies are not symmetrically located around the characteristic frequency having (in logarithmic scale) a distance equal to x and y, respectively.

Using (4), the transfer function in (1) can be alternatively written as in (5)

$$H_{IO}(s) = G_L \left(\frac{\omega_p}{\omega_z}\right) \frac{s+\omega_z}{s+\omega_p}. \tag{5}$$

The gain at high frequencies (G_H) tends to

$$G_H = G_L \left(\frac{\omega_p}{\omega_z}\right) = G_L \left(\frac{y}{x}\right). \tag{6}$$

Setting $s = j\omega$ in (5), the derived gain and phase responses are given by (7a)–(7b), respectively

$$\mid H_{IO}(j\omega) \mid = G_L \cdot \sqrt{\frac{1+\left(\frac{\omega}{\omega_z}\right)^2}{1+\left(\frac{\omega}{\omega_p}\right)^2}}, \tag{7a}$$

$$\angle H_{IO}(j\omega) = \tan^{-1}(\omega/\omega_z) - \tan^{-1}(\omega/\omega_p). \tag{7b}$$

Generally, the *knee* frequencies of the filter are calculated from (7a) by setting the value of the gain to a desired level. The most common level is the $\pm$3dB level and this will be employed in what follows. In order to simplify the analysis, it is assumed that the pole and zero of the filter are separated in such a way that they independently determine the behavior of the filter. The asymptotic (Bode) behavior of the frequency response is determined by the relative separation between the pole and the zero of the filter. This will be also assumed hereinafter for all the types of filters which will be considered.

Type-I: $\omega_z > \omega_p$ ($x > y$ and $G_L > G_H$), then the gain response has a constant value equal to G_L until the lower *knee* frequency ω_L, which is equal to the pole frequency, and starts monotonically decreasing until the higher *knee* frequency ω_H, which is equal to the zero frequency. After this frequency, it reaches a constant value equal to G_H, due to the effect of the zero. Therefore,

$$\omega_L = \omega_p = \frac{\omega_0}{x}, \quad \omega_H = \omega_z = \frac{\omega_0}{y}. \tag{8}$$

Type-II: $\omega_p > \omega_z$ ($x < y$ or $G_L < G_H$), then the gain response has a constant value equal to G_L until the lower *knee* frequency ω_L, but now becomes equal to the zero frequency, and then it monotonically increases until reaching the higher *knee* frequency ω_H, which is now equal to the pole frequency, reaching a constant value equal to G_H. Thus,

$$\omega_L = \omega_z = \frac{\omega_0}{y}, \quad \omega_H = \omega_p = \frac{\omega_0}{x}. \tag{9}$$

Defining the geometric mean of the *knee* frequencies as the *mean* frequency (ω_m)

$$\omega_m \equiv \sqrt{\omega_L \cdot \omega_H}, \tag{10}$$

then, using (8) or (9) and (10), it is readily obtained that the relationship between the *mean* frequency and the characteristic frequency ω_0 is

$$\omega_m = \frac{\omega_0}{\sqrt{xy}}. \tag{11}$$

The gain at the *mean* frequency (G_m) is defined by (12)

$$G_m \equiv \mid H_{IO}(j\omega_m) \mid = \sqrt{G_L G_H}, \tag{12}$$

which is equal to the geometric mean of the gains at low and high frequencies.

It is now clear that the relationship between the gains at low (G_L) and high frequencies (G_H), and the gain at the *mean* frequency (G_m), is

$$G_L = G_m \sqrt{\frac{x}{y}}, \quad G_H = \frac{G_m}{\sqrt{\frac{x}{y}}}. \tag{13}$$

Therefore, the gains of the filter G_L and G_H (in dBs) are equally spaced around G_m.

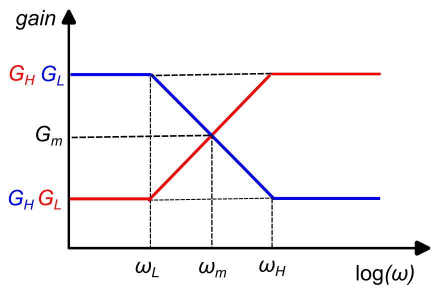

FIGURE 1. Bode plots of the gain responses of the Type-I (blue) and Type-II (red) bilinear filters, with notation of their most important frequency characteristics.

The phase at this frequency (Φ_m) reaches its minimum/maximum value given by

$$\Phi_m \equiv \angle H_{IO}(j\omega_m) = \sin^{-1}\left(\frac{1-\frac{x}{y}}{1+\frac{x}{y}}\right). \tag{14}$$

In order to facilitate the reader, the Bode plots associated with Type-I and II are demonstrated in Fig.1, where the aforementioned frequency characteristics are depicted.

B. FRACTIONAL-ORDER BILINEAR FILTERS

The pole and zero of the fractional-order filter function in (2) can be expressed as

$$\omega_p = \frac{1}{x^{1/\alpha}\tau} = \frac{\omega_0}{x^{1/\alpha}}, \quad \omega_z = \frac{1}{y^{1/\alpha}\tau} = \frac{\omega_0}{y^{1/\alpha}}, \tag{15}$$

where the distance between the pole and the zero is controlled by the order of the filter.

The transfer function in (2) can be alternatively written as

$$H_{FO}(s) = G_L\left(\frac{\omega_p}{\omega_z}\right)^{\alpha}\cdot\frac{s^{\alpha}+\omega_z^{\alpha}}{s^{\alpha}+\omega_p^{\alpha}}, \tag{16}$$

with the gain at high frequencies being

$$G_H = G_L\left(\frac{\omega_p}{\omega_z}\right)^{\alpha} = G_L\left(\frac{y}{x}\right). \tag{17}$$

Setting $s^{\alpha} = \omega^{\alpha}\cdot[\cos(0.5\alpha\pi)+j\sin(0.5\alpha\pi)]$ in (16), the gain and phase responses of the filter are given by

$$|H_{FO}(j\omega)| = G_L\cdot\sqrt{\frac{1+\left(\frac{\omega}{\omega_z}\right)^{2\alpha}+2\left(\frac{\omega}{\omega_z}\right)^{\alpha}\cos(0.5\alpha\pi)}{1+\left(\frac{\omega}{\omega_p}\right)^{2\alpha}+2\left(\frac{\omega}{\omega_p}\right)^{\alpha}\cos(0.5\alpha\pi)}}, \tag{18a}$$

$$\angle H_{FO}(j\omega) = \tan^{-1}\frac{\sin(0.5\alpha\pi)}{\left(\frac{\omega_z}{\omega}\right)^{\alpha}+\cos(0.5\alpha\pi)} - \tan^{-1}\frac{\sin(0.5\alpha\pi)}{\left(\frac{\omega_p}{\omega}\right)^{\alpha}+\cos(0.5\alpha\pi)}. \tag{18b}$$

Thus, the asymptotic behavior will be as follows:

Type-I: $\omega_z > \omega_p$ ($x > y$, $G_L > G_H$), then the filter's gain response has similar behavior as its integer-order counterpart. The difference is that the low and high *knee* frequencies are not equal to the pole/zero frequencies. They depend on the order of the filter, and they are given by

$$\omega_L = \frac{\omega_0}{x^{1/\alpha}}\cdot\left[\sqrt{1+\cos^2(0.5\alpha\pi)}-\cos(0.5\alpha\pi)\right]^{1/\alpha}, \tag{19a}$$

$$\omega_H = \frac{\omega_0}{y^{1/\alpha}}\cdot\left[\sqrt{1+\cos^2(0.5\alpha\pi)}+\cos(0.5\alpha\pi)\right]^{1/\alpha}. \tag{19b}$$

Type-II: $\omega_p > \omega_z$ ($x < y$ or $G_L < G_H$), and the frequency behavior is similar to that of the Type-II integer-order filters. The *knee* frequencies are given by (19a)–(19b) after x and y interchanging.

Using (15), it is readily obtained the relationship between the *mean* frequency (ω_m) and the characteristic frequency $\omega_0 = 1/\tau$, given by (20)

$$\omega_m = \frac{\omega_0}{(\sqrt{xy})^{1/\alpha}}. \tag{20}$$

The relationship between the low and the high frequency gains with the gain at the *mean* frequency is also given by (13) making them equally spaced around the gain at the *mean* frequency.

The phase at the *mean* frequency reaches its minimum/maximum value calculated by (21)

$$\Phi_m = \tan^{-1}\frac{\sin(0.5\alpha\pi)}{\sqrt{\frac{x}{y}}+\cos(0.5\alpha\pi)} - \tan^{-1}\frac{\sin(0.5\alpha\pi)}{\sqrt{\frac{y}{x}}+\cos(0.5\alpha\pi)}. \tag{21}$$

C. POWER-LAW BILINEAR FILTERS

The pole and zero locations of the filter in (3) are determined by (4). Thus, the transfer function in (3) becomes

$$H_{PL}(s) = G_L\left(\frac{\omega_p}{\omega_z}\right)^{\beta}\left(\frac{s+\omega_z}{s+\omega_p}\right)^{\beta}. \tag{22}$$

At high frequencies, the gain tends to the value

$$G_H = G_L\left(\frac{\omega_p}{\omega_z}\right)^{\beta} = G_L\left(\frac{y}{x}\right)^{\beta}. \tag{23}$$

The gain and phase responses of the filter are

$$|H_{PL}(j\omega)| = G_L\cdot\left[\frac{1+\left(\frac{\omega}{\omega_z}\right)^2}{1+\left(\frac{\omega}{\omega_p}\right)^2}\right]^{\beta/2}, \tag{24a}$$

$$\angle H_{PL}(j\omega) = \beta\cdot\left[\tan^{-1}(\omega/\omega_z)-\tan^{-1}(\omega/\omega_p)\right]. \tag{24b}$$

The asymptotic behavior of the filter is as follows:

Type-I: $\omega_z > \omega_p$ ($x > y$ and $G_L > G_H$), with the gain response having the same behavior as that of its fractional-order counterpart. Again, the *knee* frequencies are not equal to the pole/zero frequencies and they depend on the order of the filter with their associated expressions given by

$$\omega_L = \frac{\omega_0}{x} \cdot \sqrt{2^{1/\beta} - 1}, \quad \omega_H = \frac{\omega_0}{y} \cdot \frac{1}{\sqrt{2^{1/\beta} - 1}}. \tag{25}$$

Type-II: $\omega_p > \omega_z$ ($x < y$ and $G_L < G_H$), where the *knee* frequencies are given by (26)

$$\omega_L = \frac{\omega_0}{y} \cdot \sqrt{2^{1/\beta} - 1}, \quad \omega_H = \frac{\omega_0}{x} \cdot \frac{1}{\sqrt{2^{1/\beta} - 1}}. \tag{26}$$

The expression of the *mean* frequency, derived using (25)–(26) is the same as that which corresponds to the integer-order case, i.e., (11).

The phase, is calculated from

$$\Phi_m = \beta \cdot \sin^{-1}\left(\frac{1 - \frac{x}{y}}{1 + \frac{x}{y}}\right), \tag{27}$$

and this is the minimum/maximum value.

III. PROPOSED GENERALIZED (DOUBLE-ORDER) BILINEAR FILTERS

A. FILTERS CHARACTERISTICS

The transfer functions of the integer-order, fractional-order, and power-law bilinear filters can be generalized according to the following form

$$H_{DO}(s) = G_L \cdot \left[\frac{y(\tau s)^\alpha + 1}{x(\tau s)^\alpha + 1}\right]^\beta, \tag{28}$$

with $0 < \alpha, \beta \leq 1$ being the orders of the filter. According to (28), the integer-order, fractional-order, and power-law bilinear filters correspond to $\alpha = \beta = 1$, $\beta = 0$, and $\alpha = 0$, respectively.

The pole and zero of the filter are given by the expression in (15) and, therefore, the transfer function in (28) can be re-formed as

$$H_{DO}(s) = G_L \left(\frac{\omega_p}{\omega_z}\right)^{\alpha\beta} \left(\frac{s^\alpha + \omega_z^\alpha}{s^\alpha + \omega_p^\alpha}\right)^\beta. \tag{29}$$

Hence

$$\frac{G_L}{G_H} = \left(\frac{\omega_z}{\omega_p}\right)^{\alpha\beta} = \left(\frac{x}{y}\right)^\beta. \tag{30}$$

The resulting gain and phase responses are described by (31a)–(31b)

$$|H_{DO}(j\omega)| = G_L \left[\sqrt{\frac{1 + \left(\frac{\omega}{\omega_z}\right)^{2\alpha} + 2\left(\frac{\omega}{\omega_z}\right)^\alpha \cos(0.5\alpha\pi)}{1 + \left(\frac{\omega}{\omega_p}\right)^{2\alpha} + 2\left(\frac{\omega}{\omega_p}\right)^\alpha \cos(0.5\alpha\pi)}}\right]^\beta, \tag{31a}$$

$$\angle H_{DO}(j\omega) = \beta \cdot \left\{\tan^{-1}\frac{\sin(0.5\alpha\pi)}{\left(\frac{\omega_z}{\omega}\right)^\alpha + \cos(0.5\alpha\pi)} - \tan^{-1}\frac{\sin(0.5\alpha\pi)}{\left(\frac{\omega_p}{\omega}\right)^\alpha + \cos(0.5\alpha\pi)}\right\}. \tag{31b}$$

TABLE 1. Frequency characteristics of double-order bilinear filters.

Variable	Expression
ω_p	$\omega_0/x^{1/\alpha}$
ω_z	$\omega_0/y^{1/\alpha}$
ω_L †	$\frac{\omega_0}{x^{1/\alpha}} \cdot \left[\sqrt{2^{1/\beta} - 1 + \cos^2(0.5\alpha\pi)} - \cos(0.5\alpha\pi)\right]^{1/\alpha}$
ω_H †	$\frac{\omega_0}{y^{1/\alpha}} \cdot \left[\sqrt{2^{1/\beta} - 1 + \cos^2(0.5\alpha\pi)} - \cos(0.5\alpha\pi)\right]^{-1/\alpha}$
G_H	$G_L(y/x)^\beta$
ω_m	$\omega_0/(\sqrt{xy})^{1/\alpha}$
Φ_m	from (33)

†In the case of Type-II filters, x and y must be interchanged.

The shape of the asymptotic behaviors of the filter is the same as that of Type-I and Type-II kinds, with the *knee* frequencies given by the expressions in (32a)–(32b)

$$\omega_L = \frac{\omega_0}{x^{1/\alpha}} \cdot \left[\sqrt{2^{1/\beta} - 1 + \cos^2(0.5\alpha\pi)} - \cos(0.5\alpha\pi)\right]^{1/\alpha}, \tag{32a}$$

$$\omega_H = \frac{\omega_0}{y^{1/\alpha}} \cdot \left[\sqrt{2^{1/\beta} - 1 + \cos^2(0.5\alpha\pi)} - \cos(0.5\alpha\pi)\right]^{-1/\alpha}, \tag{32b}$$

for the Type-I and with the same expressions for Type II after interchanging x and y.

The expression of the *mean* frequency of the filter is also given by (20), while the phase reaches its minimum/maximum value calculated by (33)

$$\Phi_m = \beta \cdot \left\{\tan^{-1}\frac{\sin(0.5\alpha\pi)}{\sqrt{\frac{x}{y}} + \cos(0.5\alpha\pi)} - \tan^{-1}\frac{\sin(0.5\alpha\pi)}{\sqrt{\frac{y}{x}} + \cos(0.5\alpha\pi)}\right\}. \tag{33}$$

The most important frequency characteristics of the generalized bilinear filter are summarized in Table 1. It must be mentioned at this point that the frequency characteristics of the integer-order filters ($\alpha = \beta = 1$), fractional-order ($\beta = 0$), and power-law ($\alpha = 0$) bilinear filers could be readily obtained from this Table.

In order to demonstrate the design flexibility offered by the double-order filter, for a given set of values $\{x, y, G_L, \omega_0\}$ the control of the frequency characteristics of the filter is described in Table 2. Considering the extra degrees of freedom $\{\alpha, \beta\}$ in the case of the double-order filter, it is evident from this Table that the five characteristics are controlled by five parameters, offering the highest possible freedom to the designer.

B. REALIZATION OF THE PROPOSED GENERALIZED BILINEAR FILTER

1) MINIMUM ACTIVE COMPONENT COUNT REALIZATION

Let us consider the structure in Fig.2a where a CFOA has been chosen as the active element [7]. The realized transfer

TABLE 2. Controllability of the frequency characteristics of integer-order (I-O), fractional-order (F-O), power-law (P-L) and double-order (D-O) bilinear filters.

Variable	I-O	F-O	P-L	D-O
pole/zero freq. (ω_p/ω_z)	fixed	α	fixed	α
knee freq. (ω_L, ω_H)	fixed	α	β	α, β
gain at high-freq. (G_H)	fixed	fixed	β	β
mean freq. (ω_m)	fixed	α	fixed	α
phase at *mean* freq. (Φ_m)	fixed	α	β	α, β

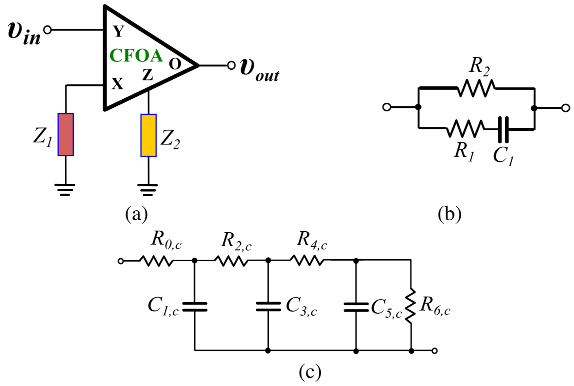

FIGURE 2. (a) CFOA based generalized structure for implementing integer and non-integer order bilinear filter functions, (b) RC network for implementing Z_2 for Type-I or Z_1 for Type-II integer-order filters, and (c) Cauer-I RC network for implementing Z_2 for Type-I or Z_1 for Type-II generalized non-integer order bilinear filters.

function is

$$H(s) = \frac{Z_2}{Z_1}. \tag{34}$$

Assuming that the impedance Z_2 is realized by the network in Fig.2b, its value is given by

$$Z_2(s) = R_2 \frac{R_1 C_1 s + 1}{(R_1 + R_2) C_1 s + 1}. \tag{35}$$

Using (34)–(35) and considering that $Z_1 = R_3$, then the following transfer function is readily obtained

$$H_{IO-I}(s) = \frac{R_2}{R_3} \frac{R_1 C_1 s + 1}{(R_1 + R_2) C_1 s + 1}. \tag{36}$$

Comparing (1) and (36), it is derived that: $G_L = R_2/R_3$, and $x/y = 1 + R_2/R_1 > 1$. Therefore, this topology implements the Type-I integer-order bilinear transfer function. The values of x and y depend on the determination of the time constant. For example:

- Assuming that $\tau = RC_1$, then $x = (R_1 + R_2)/R$ and $y = R_1/R$, with R being an arbitrary value resistor.
- Assuming that $\tau = \tau_z = R_1 C_1$ (i.e., equal to the time constant associated with the zero frequency), then $x = 1 + R_2/R_1$ and $y = 1$.
- Assuming that $\tau = \sqrt{\tau_p \tau_z} = \sqrt{R_1(R_1 + R_2)} C_1$ (i.e., equal to the geometric mean of the time constants associated with the pole and zero frequencies), then $x = 1/y = \sqrt{1 + R_2/R_1}$. This choice establishes that the *mean* frequency will be equal to the characteristic frequency ($\omega_m = \omega_0$) and that the pole and zero frequencies will be symmetrically located around the *mean* frequency.

The corresponding Type-II filters are implemented by interchanging the position of the network that implements Z_2 in the previous case with the position of R_3. As a result, and since (34) is still valid, the transfer function becomes

$$H_{IO-II}(s) = \frac{R_3}{R_2} \frac{(R_1 + R_2) C_1 s + 1}{R_1 C_1 s + 1}, \tag{37}$$

where it is obvious that $x < y$, and the aforementioned possible choices of the characteristic frequency are still valid.

The realization of the corresponding fractional-order Type-I and Type-II bilinear filters could be performed by substituting the capacitor in Fig.2b by its fractional-order counterpart. The approximation of its impedance $Z_\alpha = 1/C_\alpha s^\alpha$ can be performed by Foster or Cauer RC networks [8]. However, the realization of the power-law and double-order filters can not be performed by this way, due to the presence of non-integer orders that are not directly associated with Laplacian operators.

Therefore, Type-I bilinear non-integer order filter (i.e., fractional-order, power-law, and double-order) will be realized by assuming that

$$Z_2(s) = R H_{DO}(s) = R G_L \left[\frac{y(\tau s)^\alpha + 1}{x(\tau s)^\alpha + 1} \right]^\beta, \quad Z_1 = R, \tag{38}$$

while for the Type-II

$$Z_2 = R, \quad Z_1(s) = \frac{R}{H_{DO}(s)} = \frac{R}{G_L} \left[\frac{x(\tau s)^\alpha + 1}{y(\tau s)^\alpha + 1} \right]^\beta. \tag{39}$$

Employing a 3$^{\text{rd}}$-order approximation and using the curve-fitting based approximation employed also in [9], the frequency dependent impedances in (38)–(39) are approximated by the transfer function in (40)

$$Z_{approx}(s) \simeq \frac{B_3 s^3 + B_2 s^2 + B_1 s + B_0}{s^3 + A_2 s^2 + A_1 s + A_0}, \tag{40}$$

with A_i and B_j ($i = 0, 1, 2,\ j = 0, 1, 2, 3$) being positive and real coefficients.

Considering, for example, the Cauer-I network demonstrated in Fig.2c, the continued fraction expansion of (40) takes the form

$$Z_{approx}(s) = q_0 + \cfrac{1}{q_1 s + \cfrac{1}{q_2 + \cfrac{1}{q_3 s + \cfrac{1}{q_4 + \cfrac{1}{q_5 s + q_6}}}}}, \tag{41}$$

and the design equations will be given by (42)

$$R_{0,c} = q_0 \quad C_{i,c} = q_i \quad R_{j,c} = q_j \quad i = 1, 3, 5 \ldots \quad j = 2, 4, 6 \tag{42}$$

where $q_{i(j)}$ are the coefficients of the continued fraction expansion in (41).

2) PROGRAMMABLE REALIZATION

The programmability of the proposed bilinear filter functions can be achieved as follows: starting from the transfer function in (28) and utilizing the curve-fitting based approximation (as in the previous Section), the resulting transfer function has the form

$$H_{approx}(s) \simeq \frac{D_3 s^3 + D_2 s^2 + D_1 s + D_0}{s^3 + C_2 s^2 + C_1 s + C_0}, \tag{43}$$

with C_i and D_j ($i = 0, 1, 2,\ j = 0, 1, 2, 3$) being also positive and real coefficients. The transfer function in (43) can be implemented by a multi-feedback structure described by the transfer function in (44)

$$C_{FLF}(s) = \frac{G_3 s^3 + \frac{G_2}{\tau_1} s^2 + \frac{G_1}{\tau_1 \tau_2} s + \frac{G_0}{\tau_1 \tau_2 \tau_3}}{s^3 + \frac{1}{\tau_1} s^2 + \frac{1}{\tau_1 \tau_2} s + \frac{1}{\tau_1 \tau_2 \tau_3}}. \tag{44}$$

The scaling factors and the time constants are calculated by equating the coefficients of (43) and (44).

The transfer function in (44) can be implemented using Operational Transconductance Amplifiers (OTAs) as active elements, with their small-signal electronically controlled transconductance parameter used for implementing the scaling factors and time constants [7]. Another alternative is the utilization of an FPAA device such as the Anadigm AN231E04 device, where the programmability is achieved through the utilization of the switched-capacitor technique [10], [11].

IV. APPLICATION DESIGN EXAMPLES

The transfer functions of integer-order, fractional-order, and power-law compensators are the following

$$H_{IO,C}(s) = G_L \cdot \frac{\tau s + 1}{x \tau s + 1}, \tag{45}$$

$$H_{FO,C}(s) = G_L \cdot \frac{(\tau s)^\alpha + 1}{x (\tau s)^\alpha + 1}, \tag{46}$$

$$H_{PL,C}(s) = G_L \cdot \left(\frac{\tau s + 1}{x \tau s + 1}\right)^\beta. \tag{47}$$

Therefore, compensators are a special case of bilinear filters with $y = 1$. In the case that $x > 1$, this is a Type-I compensator known as lag-compensator, while for $x < 1$ the resulting Type-II compensator is known as lead-compensator [1], [2], [12], [13], [14], [15], [16], [17], [18], [19], [20], [21].

The corresponding expressions of shelving filters are

$$H_{IO,SF}(s) = H_{SF}(s) = G_L \cdot \frac{\frac{\tau s}{x} + 1}{x \tau s + 1}, \tag{48}$$

$$H_{FO,SF}(s) = G_L \cdot \frac{\frac{(\tau s)^\alpha}{x} + 1}{x (\tau s)^\alpha + 1}, \tag{49}$$

$$H_{PL,SF}(s) = G_L \cdot \left(\frac{\frac{\tau s}{x} + 1}{x \tau s + 1}\right)^\beta. \tag{50}$$

Consequently, shelving filters are a special case of their corresponding bilinear filter counterparts, with $x = 1/y$. Thus, the case of Type-I shelving filters corresponds to $x > 1$, and these are known as low-shelving filters, while for $x < 1$, the resulting Type-II shelving filters are known as high-shelving filters [3], [22], [23], [24].

Concluding, shelving filters and compensators are different aspects of the same core, which is a bilinear filter. In other words, having available a bilinear filter structure, it can behave like a shelving filter or a compensator by choosing suitable values of the pole/zero frequencies. The only difference between shelving filters and compensators is related to the considered frequency range; shelving filters are employed for applications in the acoustic range (i.e., 20Hz–20kHz), while compensators are employed in control applications in the range of Hz. In other words, the difference is in the location of the *mean* frequency or, equivalently, in the location of the characteristic frequency ω_0.

The transfer functions of the proposed compensators and shelving filters will be

$$H_{DO,C}(s) = G_L \cdot \left[\frac{(\tau s)^\alpha + 1}{x (\tau s)^\alpha + 1}\right]^\beta, \tag{51}$$

$$H_{DO,SF}(s) = G_L \cdot \left[\frac{\frac{(\tau s)^\alpha}{x} + 1}{x (\tau s)^\alpha + 1}\right]^\beta, \tag{52}$$

respectively, offering the aforementioned benefits in terms of design flexibility and circuit complexity.

A. DESIGNS OF COMPENSATORS

Assuming for instance $\omega_0 = 10 rad/s$, the range of approximation $(10^{-2}\omega_0, 10^{+2}\omega_0)$, and $R = 10k\Omega$, then the values of passive elements (rounded to the E96 series defined in IEC 60063 standard) which are required for implementing the considered Type-I non-integer order compensators with $G_L = 20dB$ and $x = 1/y = 3.162$, are summarized in Table 3a. The corresponding values in the case of Type-II compensators with $G_L = 0dB$ and $x = 1/y = 0.3162$, are provided in Table 3b. The values of the passive elements $\{R_1, R_2, R_3, C_1\}$, which correspond to the case of integer-order compensators, are $\{10k\Omega, 100k\Omega, 10k\Omega, 3.01\mu F\}$ and $\{1.1k\Omega, 10k\Omega, 10k\Omega, 28.7\mu F\}$ for Types-I and II, respectively.

The performance of bilinear compensators is evaluated using the OrCAD PSpice suite, with the AD844 discrete component biased at ±10V employed as CFOA. Using the component values in Table 3, the simulated responses are depicted in Fig.3, where the theoretical plots are also provided by dashes. The most important performance characteristics of the non-integer order filters are summarized in Table 4, accompanied by the theoretically predicted values given in parentheses. The corresponding results in the case of Type-I integer-order compensators are 3.13(3.19)rad/s, 27.43(31.29)rad/s, 9.3(10)rad/s, 10(10)dB, and $-55.9^o(-54.9^o)$, while for the Type-II the results are 3.22(3.19)rad/s, 32.98(31.29)rad/s, 10.3(10)rad/s, 10.2(10)dB, and $54.3^o(54.9^o)$.

TABLE 3. Values of the RC-network in Fig.1c for implementing (a) Type-I, and (b) Type-II non-integer order compensators.

Element	F-O ($\alpha = 0.8$)	P-L ($\beta = 0.8$)	D-O ($\alpha = \beta = 0.8$)
$R_{0,c}$ (kΩ)	10.7	15.8	16.5
$R_{2,c}$ (kΩ)	26.1	60.4	26.1
$R_{4,c}$ (kΩ)	43.2	20	38.3
$R_{6,c}$ (kΩ)	17.4	3.24	16.2
$C_{1,c}$ (μF)	2.37	2.8	1.87
$C_{3,c}$ (μF)	4.02	4.75	4.02
$C_{5,c}$ (μF)	54.9	53.6	51.1

(a)

Element	F-O ($\alpha = 0.8$)	P-L ($\beta = 0.8$)	D-O ($\alpha = \beta = 0.8$)
$R_{0,c}$ (kΩ)	1.02	1.58	1.62
$R_{2,c}$ (kΩ)	1.33	6.04	1.62
$R_{4,c}$ (kΩ)	3.92	1.96	3.65
$R_{6,c}$ (kΩ)	3.16	0.402	2.67
$C_{1,c}$ (μF)	19.1	28	15.8
$C_{3,c}$ (μF)	21.5	44.2	23.2
$C_{5,c}$ (μF)	130	392	162

(b)

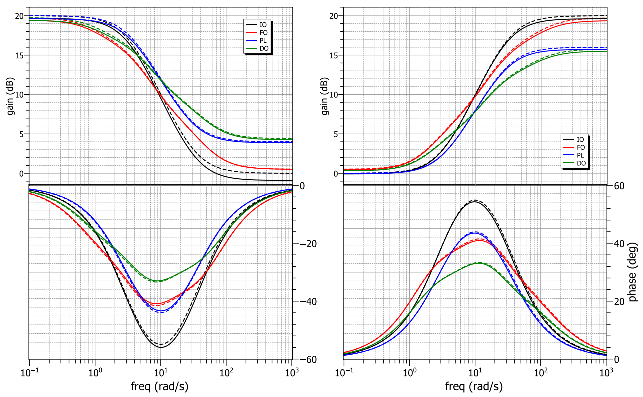

(a) (b)

FIGURE 3. Simulated gain and phase responses of (a) Type-I and (b) Type-II integer-order, fractional-order, power-law, and double-order compensators implemented using the structure in Fig.2.

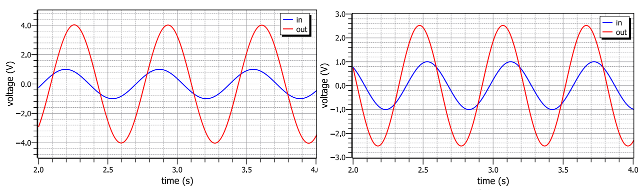

(a) (b)

FIGURE 4. Time-domain behavior of (a) Type-I, and (b) Type-II double-order compensators stimulated at their *mean* frequency by a $2V_{p\text{-}p}$ sinusoidal input.

The time-domain behavior is evaluated in the case of Type-I and II double-order compensators. For this purpose, they are stimulated by a 2Vpeak-to-peak sinusoidal signal at their *mean* frequency. According to the waveforms in Fig.4a, the gain and the phase difference between the output and input waveforms are equal to {12.1dB, -32.9^{o}} for the Type-I, with the associated theoretical values being {12dB, -33.09^{o}}. The simulated values in the case of the Type-II compensator, derived from Fig.4b, are {8.04dB, 33.6^{o}} close to the theoretically predicted ones {8dB, 33.08^{o}}.

TABLE 4. Frequency response performance characteristics of (a) Type-I, and (b) Type-II non-integer order compensators.

Variable	F-O	P-L	D-O
low *knee* freq. (rad/s)	1.59 (1.76)	3.73 (3.76)	2.03 (2.29)
high *knee* freq. (rad/s)	60 (56.74)	25.79 (26.61)	43.01 (43.72)
mean freq. (rad/s)	9.8 (10)	9.8 (10)	9.3 (10)
gain at *mean* freq. (dB)	9.9 (10)	11.9(12)	12 (12)
phase at *mean* freq. (^{o})	-40.7 (-41.4)	-43.3 (-43.9)	-32.9 (-33.1)

(a)

Variable	F-O	P-L	D-O
low *knee* freq. (rad/s)	2.09 (1.76)	3.79 (3.76)	2.29 (2.29)
high *knee* freq. (rad/s)	51.23 (56.69)	27.67 (26.61)	48.36 (43.72)
mean freq. (rad/s)	10.3 (10)	10.2 (10)	10.5 (10)
gain at *mean* freq. (dB)	9.9 (10)	8.1 (8)	8 (8)
phase at *mean* freq. (^{o})	40.8 (41.4)	43.5 (43.9)	33.1 (33.1)

(b)

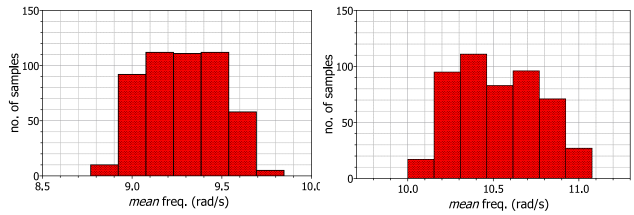

(a) (b)

FIGURE 5. Monte-Carlo analysis results about the mean frequency of (a) Type-I, and (b) Type-II double-order compensators.

TABLE 5. Values of the coefficients and time constants in (44) for implementing (a) Type-I, and (b) Type-II non-integer order shelving filters.

Variable	F-O ($\alpha = 0.8$)	P-L ($\beta = 0.8$)	D-O ($\alpha = \beta = 0.8$)
G_0	9.695	10	9.7341
G_1	6.209	5.593	6.582
G_2	2.330	2.937	3.053
G_3	1.060	1.585	1.658m
τ_1 (s)	32.988m	26.669m	38.032m
τ_2 (s)	4.171m	6.996m	4.988m
τ_3 (s)	714.190μ	1.936m	829.295μ

(a)

Variable	F-O ($\alpha = 0.8$)	P-L ($\beta = 0.8$)	D-O ($\alpha = \beta = 0.8$)
G_0	1.060	1	1.046
G_1	2.330	1.853	1.926
G_2	6.209	3.529	4.153
G_3	9.695	6.309	6.142
τ_1 (s)	140.018m	51.644m	120.584m
τ_2 (s)	23.976m	14.294m	20.047m
τ_3 (s)	3.031m	3.750m	2.629m

(b)

The sensitivity analysis is performed by employing the Monte-Carlo analysis, offered by the *Advanced Analysis* tool of the OrCAD PSpice. For this purpose, ±5% deviation from the nominal values of passive elements is assumed and the obtained histograms, for N=500 runs, of the *mean* frequency of the Type-I and II compensators are given in Fig.5. The value of the standard deviation in the case of Type-I compensator is 0.21rad/s, while for Type-II is 0.24rad/s, confirming that the presented schemes have reasonable sensitivity characteristics.

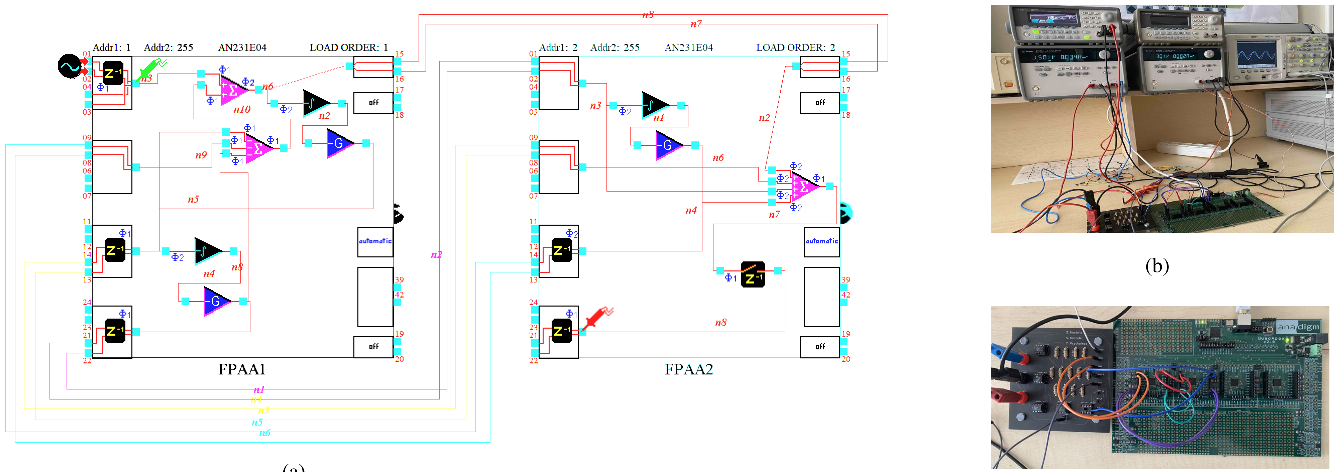

(a) (b) (c)

FIGURE 6. Implementation of the proposed generalized bilinear filter (a) Design obtained using the *Anadigm Designer*®*2* EDA software, (b) experimental setup, and (c) FPAA board with an extra board including the input and output interfaces for single-to-differential conversion and vice versa.

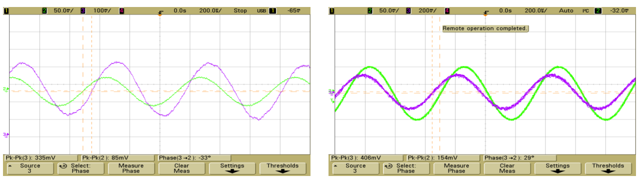

(a) (b)

FIGURE 7. Experimental time-domain behavior of (a) Type-I, and (b) Type-II double-order shelving filters stimulated at their *mean* frequency by a sinusoidal input (*green:input, magenta:output*).

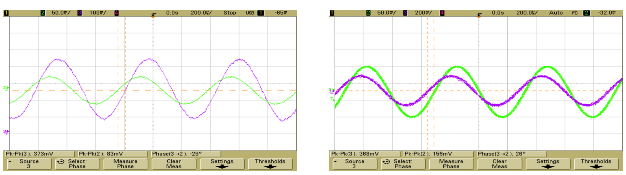

(a) (b)

FIGURE 8. Experimental demonstration of the programmability of the proposed double-order filter for ($\alpha = 0.8, \beta = 0.7$) (a) Type-I, and (b) Type-II (*green:input, magenta:output*).

B. DESIGNS OF SHELVING FILTERS

Assuming that $\omega_0 = 10^4 rad/s$ and a range of approximation $(10^{-2}\omega_0, 10^{+2}\omega_0)$, the values of the coefficients and time constants in (44) for implementing non-integer order Types-I and II shelving filters with low-frequency gains and time constant scaling factors the same as in the previous designs, are provided in Tables 5a–b, respectively. The utilized clock frequency is equal to 1MHz. Using the *Anadigm Designer*®*2* EDA software, the resulting design is demonstrated in Fig.6a, while the experimental setup is depicted in Figs.6b-c.

The gain and the input-output phase difference of the filters measured from the input-output waveforms in Fig.7, which are obtained in the cases of Type-I and Type-II double-order shelving filters stimulated by a sinusoidal signal at their *mean* frequency, are $\{11.9\text{dB}, -33^o\}$ for Type-I, and $\{8.4\text{dB}, 29^o\}$ for Type-II. The corresponding theoretical predicted values are $\{12\text{dB}, -33.08^o\}$ and $\{8\text{dB}, 33.08^o\}$.

The programmability feature of the proposed double-order filter is demonstrated for ($\alpha = 0.8, \beta = 0.7$) and ($\alpha = 0.9, \beta = 0.8$). The values of the scaling factors and

TABLE 6. Values of the coefficients and time constants in (44) for implementing (a) Type-I, and (b) Type-II double-order shelving filters with ($\alpha = 0.8, \beta = 0.7$) and ($\alpha = 0.9, \beta = 0.8$).

Variable	D-O ($\alpha = 0.8, \beta = 0.7$)	D-O ($\alpha = 0.9, \beta = 0.8$)
G_0	9.757	9.896
G_1	6.827	6.790
G_2	3.504	3.038
G_3	2.074	1.615
τ_1 (s)	40.927m	30.6250m
τ_2 (s)	5.452m	4.9912m
τ_3 (s)	892.162μ	1.052m

(a)

Variable	D-O ($\alpha = 0.8, \beta = 0.7$)	D-O ($\alpha = 0.9, \beta = 0.8$)
G_0	1.039	1.019
G_1	1.756	1.917
G_2	3.422	4.284
G_3	4.890	6.244
τ_1 (s)	112.087m	95.027m
τ_2 (s)	18.342m	20.032m
τ_3 (s)	2.443m	3.265m

(b)

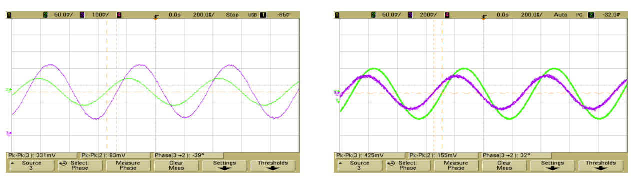

(a) (b)

FIGURE 9. Experimental demonstration of the programmability of the proposed double-order filter for ($\alpha = 0.9, \beta = 0.8$) (a) Type-I, and (b) Type-II (*green:input, magenta:output*).

time constants for implementing the resulting approximation transfer functions are given in Table 6. The time-domain behavior of these filters is demonstrated in Fig.8 for the first case, while Fig.9 corresponds to the second one. In both cases, the filters are stimulated by a sinusoidal signal at their *mean* frequency. The values of the gain and phase are {13.04dB, -29^o} for the Type-I and {7.46dB, 26^o} for the Type-II filters with ($\alpha = 0.8, \beta = 0.7$), when the corresponding theoretical values are {13dB, -28.95^o} and {7dB, 28.95^o}. Respectively, when ($\alpha = 0.9, \beta = 0.8$), the measured values of gain and phase are {12.02dB, -39^o} for Type-I and {8.76dB, 32^o} for Type-II double-order shelving filters, when the corresponding theoretical predicted values are equal to {12dB, -38.28^o} and {8dB, 38.28^o}.

V. CONCLUSION

Bilinear filters are applicable in control systems as lead/lag-compensators and in acoustic systems as low/high-shelving filters. The employment of non-integer orders in their transfer functions offers design flexibility but, in general, suffers from the increased circuit complexity. The proposed double-order bilinear filter function offers the most economical solution in terms of the active component count, while the presented FPAA based implementation offers programmability. All possible non-integer order versions (i.e., fractional-order, power-law, and double-order) are implementable by the same core, just by interchanging the impedances in the case of active RC implementation, or adjusting the coefficients of the approximation transfer function. Future research plans include exploring double-order PID controllers, which generalize fractional-order controllers.

ACKNOWLEDGMENT

The publication of the article in OA mode was financially supported by HEAL-Link.

REFERENCES

[1] C. Mu niz-Montero, L. A. Sánchez-Gaspariano, C. Sánchez-López, V. R. González-Díaz, and E. Tlelo-Cuautle, "On the electronic realizations of fractional-order phase-lead-lag compensators with OpAmps and FPAAs," in *Fractional Order Control and Synchronization of Chaotic Systems*. Berlin, Germany: Springer, 2017, pp. 131–164.

[2] S. Kapoulea, G. Tsirimokou, C. Psychalinos, and A. S. Elwakil, "OTA-C implementation of fractional-order lead/lag compensators," in *Proc. Novel Intell. Lead. Emerg. Sci. Conf. (NILES)*, vol. 1, Oct. 2019, pp. 38–41.

[3] S. Kapoulea, A. Yesil, C. Psychalinos, S. Minaei, A. S. Elwakil, and P. Bertsias, "Fractional-order and power-law shelving filters: Analysis and design examples," *IEEE Access*, vol. 9, pp. 145977–145987, 2021.

[4] F. Sen, A. Kircay, B. Sonbas Cobb, and H. Karci, "Current-mode fractional-order shelving filters using MCFOA for acoustic applications," *Int. J. Electron. Commun.*, vol. 163, May 2023, Art. no. 154608.

[5] J. Nako, C. Psychalinos, A. S. Elwakil, and S. Minaei, "Non-integer order generalized filters designs," *IEEE Access*, vol. 11, pp. 116846–116859, 2023.

[6] Anadigm. *AN231E04 dpASP: The AN231E04 dpASP Dynamically Reconfigurable Analog Signal Processor*. Accessed: Jan. 24, 2024. [Online]. Available: https://www.anadigm.com/an231e04.asp

[7] J. Nako, C. Psychalinos, A. S. Elwakil, and D. Jurisic, "Design of higher-order fractional filters with fully controllable frequency characteristics," *IEEE Access*, vol. 11, pp. 43205–43215, 2023.

[8] G. Tsirimokou, "A systematic procedure for deriving RC networks of fractional-order elements emulators using MATLAB," *Int. J. Electron. Commun.*, vol. 78, pp. 7–14, Aug. 2017.

[9] S. Kapoulea, C. Psychalinos, and A. S. Elwakil, "Power law filters: A new class of fractional-order filters without a fractional-order Laplacian operator," *Int. J. Electron. Commun.*, vol. 129, Feb. 2021, Art. no. 153537.

[10] E. Tlelo-Cuautle, A. D. Pano-Azucena, O. Guillén-Fernández, and A. Silva-Juárez, "Analog implementations of fractional-order chaotic systems," in *Analog/Digital Implementation of Fractional Order Chaotic Circuits and Applications*. Cham, Switzerland: Springer, 2020, pp. 93–114.

[11] A. M. Hassanein, A. H. Madian, A. G. G. Radwan, and L. A. Said, "On the design flow of the fractional-order analog filters between FPAA implementation and circuit realization," *IEEE Access*, vol. 11, pp. 29199–29214, 2023.

[12] C. A. Monje, A. J. Calderon, B. M. Vinagre, and V. Feliu, "The fractional order lead compensator," in *Proc. 2nd IEEE Int. Conf. Comput. Cybern. (ICCC)*, Aug./Sep. 2004, pp. 347–352.

[13] C. Yeroglu and N. Tan, "Classical controller design techniques for fractional order case," *ISA Trans.*, vol. 50, no. 3, pp. 461–472, Jul. 2011.

[14] M. S. Tavazoei and M. Tavakoli-Kakhki, "Compensation by fractional-order phase-lead/lag compensators," *IET Control Theory Appl.*, vol. 8, no. 5, pp. 319–329, Mar. 2014.

[15] M. C. Boskovic, M. R. Rapaic, T. B. Sekara, P. D. Mandic, M. P. Lazarevic, B. Cvetkovic, B. Lutovac, and M. Dakovic, "On the rational representation of fractional order lead compensator using Padé approximation," in *Proc. 7th Medit. Conf. Embedded Comput. (MECO)*, Jun. 2018, pp. 1–4.

[16] A. A. Dastjerdi, B. M. Vinagre, Y. Chen, and S. H. HosseinNia, "Linear fractional order controllers; a survey in the frequency domain," *Annu. Rev. Control*, vol. 47, pp. 51–70, Apr. 2019.

[17] G. Maione, "Design of cascaded and shifted fractional-order lead compensators for plants with monotonically increasing lags," *Fractal Fractional*, vol. 4, no. 3, p. 37, Jul. 2020.

[18] A. Tepljakov, B. B. Alagoz, C. Yeroglu, E. A. Gonzalez, S. H. Hosseinnia, E. Petlenkov, A. Ates, and M. Cech, "Towards industrialization of FOPID controllers: A survey on milestones of fractional-order control and pathways for future developments," *IEEE Access*, vol. 9, pp. 21016–21042, 2021.

[19] I. Petráš, *Handbook of Fractional Calculus with Applications*, no. 6. Berlin, Germany: De Gruyter, 2019.

[20] P. Prommee and P. Pienpichayapong, "Reconfigurable fractional-order operator and bandwidth expansion suitable for PI^α controller," *IEEE Trans. Ind. Electron.*, vol. 71, no. 5, pp. 5126–5136, May 2024.

[21] G. Avon, R. Caponetto, E. Murgano, and M. G. Xibilia, "Implementation of a fully analog feedback loop with a carbon-black-based fractional order controller," *ISA Trans.*, vol. 135, pp. 105–114, Apr. 2023.

[22] S. Sarkka and A. Huovilainen, "Accurate discretization of analog audio filters with application to parametric equalizer design," *IEEE Trans. Audio, Speech, Language Process.*, vol. 19, no. 8, pp. 2486–2493, Nov. 2011.

[23] V. Välimäki and J. Reiss, "All about audio equalization: Solutions and frontiers," *Appl. Sci.*, vol. 6, no. 5, p. 129, May 2016.

[24] G. A. Haidar, R. A. Z. Daou, and X. Moreau, "Synthesis of a fractional order audio boost filter," in *Proc. 29th Int. Conf. Microelectron. (ICM)*, Dec. 2017, pp. 1–5.

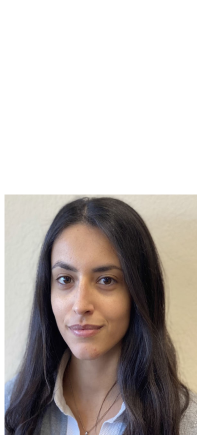

JULIA NAKO (Graduate Student Member, IEEE) received the B.Sc. and M.Sc. degrees from the University of Patras, Greece, in 2021 and 2023, respectively, where she is currently pursuing the Ph.D. degree with the Postgraduate Studies Program "Electronics-Circuits and Systems," Physics Department. She is a member of the Analog VLSI Design Team, Electronics Laboratory, working under the supervision of Prof. Costas Psychalinos. Her current research interests include the design of analog integrated circuits and systems for signal processing, including non-integer order circuits, control systems, and biomedical circuits.

COSTAS PSYCHALINOS (Senior Member, IEEE) received the B.Sc. and Ph.D. degrees in physics and electronics from the University of Patras, Greece, in 1986 and 1991, respectively. From 1993 to 1995, he was a Postdoctoral Researcher with the VLSI Design Laboratory, University of Patras. From 1996 to 2000, he was an Adjunct Lecturer with the Department of Computer Engineering and Informatics, University of Patras. From 2000 to 2004, he was an Assistant Professor with the Electronics Laboratory, Department of Physics, Aristotle University of Thessaloniki, Greece. Since 2004, he has been a Faculty Member of the Electronics Laboratory, Department of Physics, University of Patras, where he is currently a Full Professor. His current research interests include the development of CMOS analog integrated circuits, including fractional-order circuits and systems, continuous and discrete-time analog filters, amplifiers, and low voltage/low power building blocks for analog signal processing. He is a member of the Nonlinear Circuits and Systems Technical Committee of the IEEE CAS Society. He serves as the Editor-in-Chief for the Circuit and Signal Processing Section of the *Electronics* journal (MDPI). He serves as an Area Editor for *International Journal of Electronics and Communications* (AEUE) journal and an Editor for *International Journal of Circuit Theory and Applications*. He is an Associate Editor of *Circuits Systems and Signal Processing* journal and *Journal of Advanced Research*. He is a member of the editorial board of the *Microelectronics Journal*, *Analog Integrated Circuits and Signal Processing Journal*, *IETE Journal of Education*, *Fractal and Fractional* journal, and *Journal of Low Power Electronics and Applications*.

FABIAN KHATEB received the M.Sc. degree in electrical engineering and communication, the M.Sc. degree in business and management, the Ph.D. degree in electrical engineering and communication, and the Ph.D. degree in business and management from the Brno University of Technology, Czech Republic, in 2002, 2003, 2005, and 2007, respectively. He is currently a Professor with the Department of Microelectronics, Faculty of Electrical Engineering and Communication, Brno University of Technology; the Department of Electrical Engineering, University of Defence, Brno; and the Department of Information and Communication Technology in Medicine, Faculty of Biomedical Engineering, Czech Technical University in Prague. He holds five patents. He has authored or coauthored over 140 publications in journals and proceedings of international conferences. His expertise is in new principles of designing low-voltage low-power analog circuits, particularly for biomedical applications. He is a member of the editorial board of *Microelectronics Journal*, *Sensors*, *Machines*, *Electronics*, and *Journal of Low Power Electronics and Applications*. He is an Associate Editor of IEEE Access, *Circuits, Systems and Signal Processing*, *IET Circuits, Devices and Systems*, and *International Journal of Electronics*. He was a Lead Guest Editor for the Special Issues on Low Voltage Integrated Circuits and Systems of *Circuits, Systems and Signal Processing*, in 2017, *IET Circuits Devices and Systems*, in 2018, and *Microelectronics Journal*, in 2019. He was also a Guest Editor for the Special Issue on Current-Mode Circuits and Systems: Recent Advances, Design and Applications of *International Journal of Electronics and Communications*, in 2017.

AHMED S. ELWAKIL (Senior Member, IEEE) was born in Cairo, Egypt. He received the B.Sc. and M.Sc. degrees in electronics and communications from Cairo University, Egypt, and the Ph.D. degree in electrical and electronic engineering from the National University of Ireland, University College Dublin. He also held visiting positions at Istanbul Technical University, Turkey; Queens University, Belfast, U.K.; the Technical University of Denmark, Lyngby, Denmark; and the King Abdullah University of Science and Technology, Saudi Arabia. He is currently a Full Professor with the University of Sharjah, United Arab Emirates; the University of Calgary, AB, Canada; and the Nanoelectronics Integrated Systems Center (NISC) Research Center, Nile University, Cairo. He has authored or coauthored more than 350 publications in these areas (current H-index 45). His research interests include circuit theory, nonlinear dynamics, chaos theory, and fractional-order circuits and systems with diverse applications ranging from the modeling of oscillatory networks and nonlinear behavior in electronic circuits and plasma physics to modeling of energy storage devices, bio-materials, and biological tissues. He has been a member of the IEEE Technical Committee on Nonlinear Circuits and Systems, since 2000. He was a recipient of the Egyptian Government First Class Medal for achievements in engineering sciences, in 2015, and the UAE President Award (Khalifa Award), in 2020. He is an International Observer in the European Cooperation in Science and Technology (COST) action on fractional-order system analysis synthesis and their importance for future design (CA15225) and an Expert with the United Nations Development Program (UNDP). He was on the editorial board of IEEE Journal on Emerging and Selected Topics in Circuits and Systems and an Associate Editor of IEEE Transactions on Circuits and Systems—I: Regular Papers. He currently serves as the Editor-in-Chief for the *International Journal of Circuit Theory and Applications* (Wiley) and an Associate Editor for *International Journal of Electronics and Telecommunications* (AEUE, Elsevier).